High-order finite elements for the solution of Helmholtz problems ☆

K. Christodoulou [a], O. Laghrouche [a,*], M.S. Mohamed [a], J. Trevelyan [b]

[a] Institute for Infrastructure and Environment, Heriot-Watt University, Edinburgh EH14 4AS, UK
[b] School of Engineering and Computing Sciences, Durham University, Durham DH1 3LE, UK

ARTICLE INFO

ABSTRACT

In this paper, two high-order finite element models are investigated for the solution of two-dimensional wave problems governed by the Helmholtz equation. Plane wave enriched finite elements, developed in the Partition of Unity Finite Element Method (PUFEM), and high-order Lagrangian-polynomial based finite elements are considered. In the latter model, the Chebyshev-Gauss-Lobatto nodal distribution is adopted and the approach is often referred to as the Spectral Element Method (SEM). The two strategies, PUFEM and SEM, were developed separately and the current study provides data on how they compare for solving short wave problems, in which the characteristic dimension is a multiple of the wavelength. The considered test examples include wave scattering by a rigid circular cylinder, evanescent wave cases and propagation of waves in a duct with rigid walls. The two approaches are assessed in terms of accuracy for increasing SEM order and PUFEM enrichment. The conditioning, discretization level, total number of storage locations and total number of non-zero entries are also compared.

© 2017 Published by Elsevier Ltd.

1. Introduction

The finite element method has been used for decades as a numerical tool for solving various engineering wave problems thanks to its ability to deal with complexities related to geometry and material properties. For practical ease, low order polynomial based elements have been employed and these require the use of many nodal points per wavelength to achieve acceptable accuracy. Usually, at low frequency, the known *rule of thumb* leads to use about ten nodal points per wavelength in linear elements to obtain engineering accuracy results. However, for short wave problems, as well as the discretization error the pollution error [1,11] was found to affect the solution and hence the number of nodal points per wavelength has to be further increased.

With the aim to reduce the computational cost and improve the solution accuracy, various methods based on field enrichment have been proposed. For Helmholtz wave problems, the field enrichment was carried out by incorporating plane waves or Bessel functions in the approximated wave field. Proposed methods include the least-squares method [33], the partition of unity method [18,31,30,28,20], the ultra weak variational formulation [26,27],

the generalised finite element method [44–46], the discontinuous enrichment method [6,36], the oscillated finite element polynomials [3], the stable discontinuous Galerkin method [24] and the phase reduction finite element method [7]. Enriched elements were also developed within the framework of the boundary element method such as the partition of unity boundary element method [9] or the isogeometric wave-enriched boundary element method [25]. Some of the above techniques have been extended to elastic wave problems [2,42,22], fluid–structure interaction [40], flow acoustics [37] and wave propagation in poro-elastic media [19]. For more information, the reader is directed to the reviews presented in [4] and more recently in [17].

High order polynomial based finite elements were also developed and their performance assessed for the solution of wave problems governed by the Helmholtz equation. Within the framework of the discontinuous enrichment method, two quadrilateral elements employing 16 and 32 plane waves, respectively, and featuring four and eight Lagrange multiplier degrees of freedom per edge were presented and their performance compared to that of Q4 for the solution of two-dimensional waveguide and acoustic scattering problems [12]. The construction of high order finite elements may use integrated Legendre polynomials resulting in the hierarchical *p*-FEM. Such elements were developed for the solution of three-dimensional Helmholtz problems [15] and for the case of convected wave propagation [16]. Recently, a high-order polynomial method, based on Lobatto polynomials, and the wave-based discontinuous Galerkin method are compared for the solution of

two-dimensional Helmholtz problems [23]. The use of conventional Lagrange polynomials were also considered to construct high order elements. These were used to solve, for example, interior acoustic problems and their performance has been assessed against high order elements with shape functions based on Bernstein polynomials [38]. Iso-geometric elements with non-uniform rational B-splines (NURBS) shape functions were also developed resulting in N-FEM. They were compared to SEM and p-FEM high order approaches for the solution of Lamb wave propagation problems [8]. High order continuous and discontinuous Galerkin methods were compared for the solution of smooth and non-smooth two dimensional scattering problems in terms of the computational cost and concluded that high order methods were more efficient [13]. In the above indicated polynomial based approaches, the order of the element shape functions is moderately high as it is considered up to the twelfth order, such as in Ref. [23].

PUFEM has been thoroughly investigated for acoustic and elastic wave problems and attempts have been made to compare its performance to that of the standard FEM [2,29]. However, in the latter references, low order elements have been considered for FEM and hence it is intended here to increase the order p to hopefully claim a fair comparison. Various families of polynomials could be considered for high order elements such as Bernstein or Lobatto polynomials [38]. These were shown to have advantages over the usual Lagrange polynomials. Indeed, elements based on high order Lagrange polynomials cannot benefit from the use of static condensation for eliminating the bubble functions to reduce the memory requirement and improve the conditioning, which is the case of the other families of high order elements mentioned above [21,39]. Despite this and for practical reasons, the considered high order elements in this paper are based on conventional Lagrange polynomials. However, they are defined on a specific nodal distribution, the Chebyshev-Gauss-Lobatto. These elements belong to the SEM family [34,35], which is a particular high order method but must not be confused with the Spectral Finite Element Method [14]. The current work assesses both PUFEM and SEM for the solution of Helmholtz problems with increasing wave numbers.

The paper is organised as follows. The next section presents the formulation of the considered Helmholtz problem. It recalls the weak form of the problem and its numerical approximation by either SEM or PUFEM. Section 3 presents numerical results for various selected problems and last, in Section 4, some concluding remarks are drawn.

2. Problem formulation and finite element models

In this section, the Helmholtz problem with Robin boundary condition is formulated and the finite element models, namely SEM and PUFEM, are presented. Let $\Omega \subset \mathbb{R}^2$ be a bounded domain with a smooth boundary Γ. For the wave field U, we assume that the time variation is such that $U(x, y, t) = u(x, y)e^{i\omega t}$ where $u = u(x, y)$ is the unknown time independent wave field, ω is the circular frequency and i stands for the complex imaginary number such that $i^2 = -1$. The Helmholtz problem for u is then defined by

$$-\Delta u - k^2 u = 0 \quad \text{in} \quad \Omega, \tag{1}$$

$$\nabla u.\mathbf{n} + iku = g \quad \text{on} \quad \Gamma. \tag{2}$$

In expressions (1) and (2), Δ is the Laplace operator, ∇ is the gradient vector and k is the wavenumber such that $\lambda = 2\pi/k$ is the wavelength. The term g represents a boundary source on Γ and $\mathbf{n}$ denotes the outward normal unit vector defined everywhere on Γ.

The weak formulation of the presented problem is obtained by multiplying the Helmholtz Eq. (1) by a smooth test function $v = v(x, y)$ and integrating over the domain Ω such that

$$-\int_\Omega (\Delta u + k^2 u)v d\Omega = 0. \tag{3}$$

Eq. (3) involves second derivatives of u. Using the integration by parts to the integrand with second order derivatives, the following equation is obtained.

$$\int_\Omega (\nabla u.\nabla v - k^2 uv)d\Omega - \oint_\Gamma (\nabla u.\mathbf{n})v \, d\Gamma = 0. \tag{4}$$

Introducing the Robin boundary condition (2), the previous expression becomes

$$\int_\Omega (\nabla u.\nabla v - k^2 uv)d\Omega + ik\oint_\Gamma uv \, d\Gamma = \oint_\Gamma gv \, d\Gamma. \tag{5}$$

The aim now is to find an approximate solution u_h of the weak form (5) using either high-order Lagrange polynomial based finite elements (SEM) or elements with plane wave enrichment (PUFEM).

2.1. SEM model

Let $M = \{\Omega_1, \ldots, \Omega_N\}$ be a partition of Ω into N uniform non-overlapping elements Ω_e, $e = 1, \ldots, N$. Each sub-domain Ω_e is given through a coordinate transformation $\mathbf{r} = L^e(\xi)$ between the real space $\mathbf{r} = (x, y)^T \in \Omega$ and the local system $\xi = (\xi, \eta)^T \in \mathcal{L}$. The sub-domains are chosen to be quadrilaterals with the geometry described by the classical 4-node interpolation functions and hence $\mathcal{L} = [-1, 1]^2$. The field unknown variable over each n-node element Ω_e is approximated by

$$u_h = \sum_{j=1}^{n} N_j u_j, \tag{6}$$

where N_j stands for the Lagrangian polynomial interpolation functions on $\mathcal{L}$ and u_j represents the nodal values corresponding to the vertices of Ω_e. The degree p of the polynomial interpolation functions N_j depends on the number of nodes assigned to the sub-domain. For example, if the approximation (6) is linear then $p = 1$ and $n = 4$. For a quadratic approximation, $p = 2$ and $n = 9$. In general, for an approximation of degree p the number of vertices per sub-domain would be $(p + 1)^2$.

For a degree p, the set $p + 1$ of Lagrange interpolation functions in one dimension are defined by

$$N_j(\xi) = \prod_{\substack{i=1 \\ i \neq j}}^{p+1} \frac{(\xi - \xi_i)}{(\xi_j - \xi_i)}, \quad j = 1, 2, \ldots, p+1, \tag{7}$$

with the property

$$N_j(\xi_i) = \begin{cases} 1, & i = j \\ 0, & i \neq j \end{cases} \quad \text{for } 1 \leqslant i, j \leqslant p+1. \tag{8}$$

For low order finite elements, it is usual and practical to use equi-spaced nodal distribution. However, it is well known that for high-order elements this distribution does not lead to good performance due to the Runge's phenomenon and hence a particular nodal distribution is adopted. As mentioned previously, high order approaches prefer other families of functions such as Bernstein or Lobatto but in this work Lagrange based high-order finite elements with the Chebyshev-Gauss-Lobatto nodal distribution are used. In one dimension and for $\xi \in [-1, 1]$, the nodal points are located at the points with

$$\xi_i = -\cos\left(\frac{(i-1)\pi}{p}\right), \quad i = 1, 2, \ldots, p+1. \tag{9}$$

Lagrange interpolation functions $N_j(\xi, \eta)$ for the two dimensional elements used in this work are easily defined by following expres-

sion (7) and in the same way the vertices locations with respect to the η coordinate can be obtained by following (9).

A Galerkin approach is used, for which the test functions are chosen such that $v = N_j$, and the resulting finite element approximation of the weak formulation (5) then reads: Find u_h of the form (6) and for all $j = 1, \ldots, (p+1) \times (p+1)$ such that

$$\int_\Omega (\nabla u_h \cdot \nabla N_j - k^2 u_h N_j) d\Omega + ik \oint_\Gamma u_h N_j d\Gamma = \oint_\Gamma g N_j d\Gamma. \tag{10}$$

For the evaluation of the integrals involved in the weak form (10), a Gauss-Legendre scheme is adopted for which a number $n_{int} = 2p - 1$ of integration points would integrate exactly polynomials of order p or less.

2.2. PUFEM model

In the PUFEM model, the sub-domains are chosen to be bi-linear quadrilaterals with the geometry described by the classical 4-node interpolation functions. At each vertex, the unknown variable u_j of expression (6) is expanded into a linear combination of q plane waves ψ_l with directions encompassing the two dimensional space. These are given by

$$\psi_l = e^{ik\mathbf{d}_l \cdot \mathbf{r}}, \tag{11}$$

with $\mathbf{d}_l = (\cos \theta_l, \sin \theta_l)^T$ and $\theta_l = 2\pi l/q$ for $l = 1, 2, \ldots, q$. The PUFEM approximation of the unknown field variable within a sub-domain Ω_e is then given by

$$u_h = \sum_{j=1}^{4} \sum_{l=1}^{q} N_j \psi_l A_j^l. \tag{12}$$

The unknowns of the problem are no more the coefficients u_j but the amplitude factors A_j^l of the plane waves. For notation convenience, the product of the linear shape function N_j and the plane wave ψ_l is written as $P_r = N_j \psi_l$, with $r = (j-1)q + l$. A Galerkin approach is also adopted here and hence taking the test function $v = P_r$. The resulting PUFEM approximation of the weak form (5) then reads: Find u_h of the form (12) and for all $r = 1, \ldots, 4q$ such that

$$\int_\Omega (\nabla u_h \cdot \nabla P_r - k^2 u_h P_r) d\Omega + ik \oint_\Gamma u_h P_r d\Gamma = \oint_\Gamma g P_r d\Gamma. \tag{13}$$

The integrals of expression (13) involve highly oscillatory functions and hence a high order Gauss-Legendre quadrature scheme is used for which the number of integration points is chosen to accommodate the multi-wavelength size of the elements. The effect of the numerical integration on the PUFEM has been investigated in past work [29,10]. As a result, the empirical expression giving the number $n_{int} = [10 \times h/\lambda] + 2$ to ensure enough integration points are used with respect to each spacial direction is adopted. It is worth noting that semi-analytical integration procedures were also developed, such as in [5,10], to reduce the computational cost but they were not used in this study.

Since Galerkin weighting is used in both weak forms (10) and (13) the global matrix of the resulting system is symmetric and block banded. A skyline storage is used with a steering vector to locate the elements and the solution is computed using a direct solver based on LDL^T decomposition where L^T is the transpose of the lower triangular matrix L and D is a diagonal matrix [32].

3. Numerical results analysis

In this section, the performance of PUFEM and SEM is first assessed for the solution of a wave scattering problem model. Then they are assessed for the solution of test problems considering evanescent waves and wave propagation in a duct with rigid walls. The assessment of both approaches is carried out for different orders p of the Lagrangian interpolation functions for SEM and different numbers q of enrichment functions for PUFEM, while the mesh is refined at high frequencies; *i.e.* the corresponding wavelength is a small fraction of a characteristic problem dimension, for example the element size h.

The performance is measured through the relative error using the L_2-norm. It is given by

$$\epsilon_2 = \frac{\|u - u_h\|_{L_2(\Omega)}}{\|u\|_{L_2(\Omega)}}, \tag{14}$$

with u being the exact solution of the considered problem and u_h the approximate solution obtained by either SEM or PUFEM. The discretization level in terms of degrees of freedom per wavelength is indicated by the parameter τ given by

$$\tau = \lambda \sqrt{\frac{totdof}{\Omega_{area}}}, \tag{15}$$

where *totdof* stands for the total number of degrees of freedom required for the solution and Ω_{area} is the area of the computational domain. Other parameters of interest, *totsys* and *totnze*, are considered which represent the total number of storage locations of the system matrix to solve and the total number of non-zero entries, respectively. Finally, the conditioning of the system matrix, denoted by κ, is also considered and is computed using the 1-norm. All computations are carried out in Fortran with double-precision complex numbers.

3.1. Wave scattering by a rigid circular cylinder

Both PUFEM and SEM models are assessed for a wave scattering problem. The computational domain is chosen to be a square of unit size defined by $\Omega = [1, 2] \times [1, 2]$. The following analytical model

$$u = -\sum_{m=0}^{\infty} i^m \varepsilon_m \frac{J'_m(ka)}{H'_m(ka)} H_m(kr) \cos m\theta \tag{16}$$

is imposed on the boundary Γ of the computational domain Ω through the source term g of expression (2). The above model (16) represents the solution of the scattering of a horizontal plane wave by a rigid circular cylinder of unit radius a centred at the origin of the Cartesian system axes. In expression (16), r and θ are the polar coordinates of a considered point, H_m and J_m are respectively the Hankel and Bessel functions of the first kind and order m, and ε_m is defined by $\varepsilon_0 = 1$, $\varepsilon_m = 2$ for all $m \geqslant 1$.

The performance of each model is measured in terms of the L_2-error ϵ_2 and by considering the discretization level τ, condition number κ, total number of storage locations *totsys* and the total number of non-zero entries *totnze*.

The wave scattering problem is solved by both approaches for the wave numbers $ka = 16\pi, 40\pi$ and 100π. For a given order p for SEM or enrichment number q for PUFEM the mesh grid is refined to carry out an h-convergence study, for each wave number case, which leads to an increase in the total number of degrees of freedom for the problem solution. For SEM, it is obvious that for low values of p we can consider many mesh refinements as low numbers of nodes are involved per element in the mesh grid, such as for $p = 10$ where many refinements are carried out, while for higher values of p less cases of mesh refinement are possible to consider similar numbers *totdof* as high numbers of nodes per element are used. This is clearly seen for $p = 50\pi$ where only two mesh grids are considered at $ka = 100\pi$.
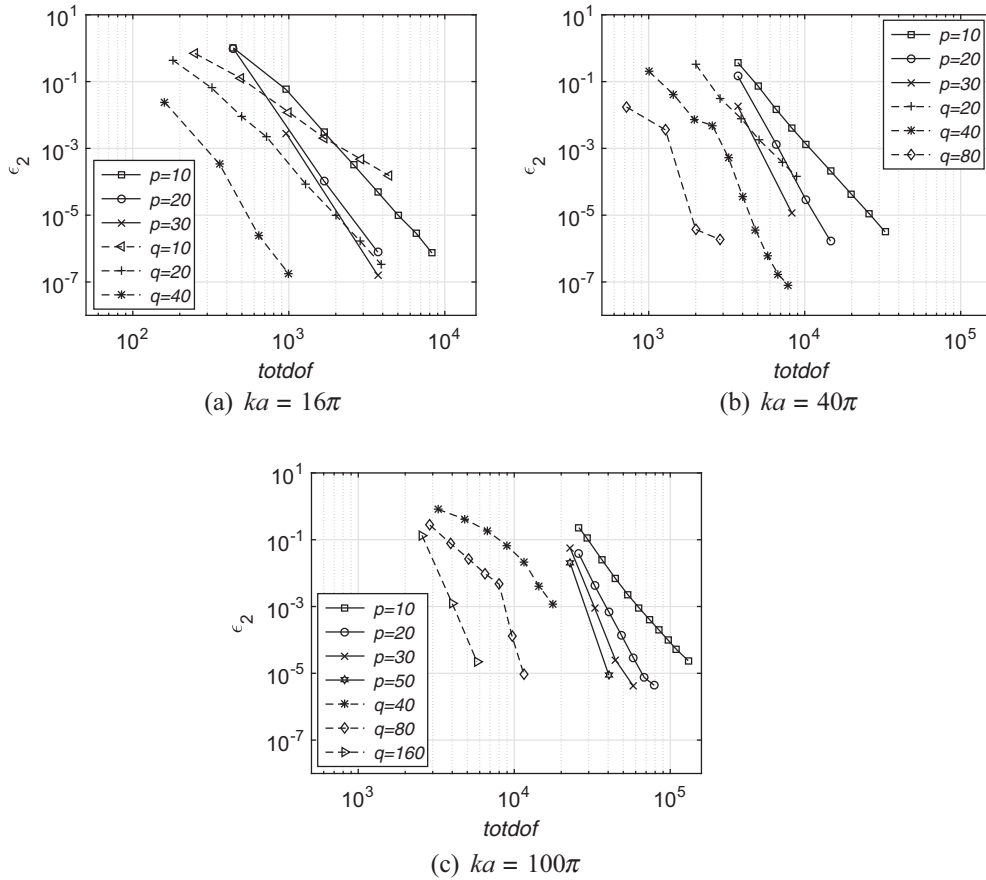
Fig. 1. Relative L_2-error for PUFEM and SEM for different values of the wave number.

The results of Fig. 1 show the values of the L_2-error for all cases of wave numbers when increasing the total number of degrees of freedom *totdof* through mesh refinements, for both approaches. For SEM, the L_2-error decreases with the increase of *totdof* at a rate which increases with the order p. This is also true for PUFEM for which the L_2-error decreases with the increase of *totdof* at a rate which increases with the number q of approximating plane waves.

For the case of $ka = 16\pi$, for example, the rate of convergence of SEM with $p = 10$ is pretty similar to the rate of convergence of PUFEM with $q = 20$. In the same way, the SEM results for $p = 20$ and 30 exhibit a similar rate shown by the results of PUFEM with $q = 40$. Looking at PUFEM with $q = 10$ and SEM with $p = 10$, we can see that PUFEM requires less degrees of freedom than SEM to achieve the same level of accuracy up to $totdof = 2 \times 10^3$, where the two lines cross each other and provide an accuracy level of $\epsilon_2 = 10^{-3}$, after which SEM requires less degrees of freedom than PUFEM to achieve the same accuracy. The same observation is made on PUFEM with $q = 20$ and SEM with $p = 30$ for which the results show a similar accuracy of, $\epsilon_2 = 10^{-5}$, around $totdof = 2 \times 10^3$. Before this crossing, PUFEM uses less degrees of freedom than SEM to provide the same level of accuracy but after the crossing SEM uses less degrees of freedom than PUFEM for the same accuracy.

The above observations also apply to the other cases of wave numbers, $ka = 40\pi$ and 100π, in the sense that increasing the order p for SEM and the number q for PUFEM leads to higher rates of convergence though for PUFEM some of the results do not show straight lines. For $ka = 40\pi$, PUFEM with $q = 20$ is shown to require less degrees of freedom than SEM with $p = 20$ to provide same quality results up to about $totdof = 7 \times 10^3$. If we increase

p to 30 while keeping $q = 20$, the crossing occurs at about $totdof = 3 \times 10^3$. For higher orders of p and higher numbers of q similar crossings may occur at very high values of *totdof* but such values are not presented in the results, especially at $ka = 100\pi$ where none of the crossings occurred.

Overall, to achieve a prescribed accuracy, it is clear that as the order p increases the total number of degrees of freedom required in the problem solution decreases. This also applies to PUFEM for which the results show that increasing the number q of enriching plane waves leads to a reduction of the required *totdof* to achieve the same accuracy. For $ka = 100\pi$, in the case of SEM, to achieve a level of accuracy of 10^{-3} about 7×10^4 degrees of freedom are required for $p = 10$. This number decreases to about 3×10^4 for $p = 50$. For PUFEM, to achieve a similar accuracy the total number of degrees of freedom is just under 2×10^4 for $q = 40$. It decreases to about 7×10^3 for $q = 80$ and to about 4×10^3 for $q = 160$. However, it is worth mentioning that while mesh refinement is practical and usual in SEM approach, for PUFEM it is preferred to keep the mesh grid unchanged and adopt further enrichment. Indeed, PUFEM and other wave-based approaches usually rely on a coarse mesh grid incorporating multi-wavelengths per nodal spacing and use increasing numbers q of enrichment functions to accommodate the highly oscillatory solutions.

The behaviour of the condition number for both SEM and PUFEM is presented in Fig. 2 for the same parameters considered in Fig. 1. For the case of SEM, the increase of κ with p or *totdof* is overall small. For PUFEM, however, κ increases sharply with *totdof*. For instance, SEM provides condition numbers in the order of 10^5 whereas PUFEM provides condition numbers which increase significantly as *totdof* increases or the number q of approximating

(a) $ka = 16\pi$ (b) $ka = 40\pi$
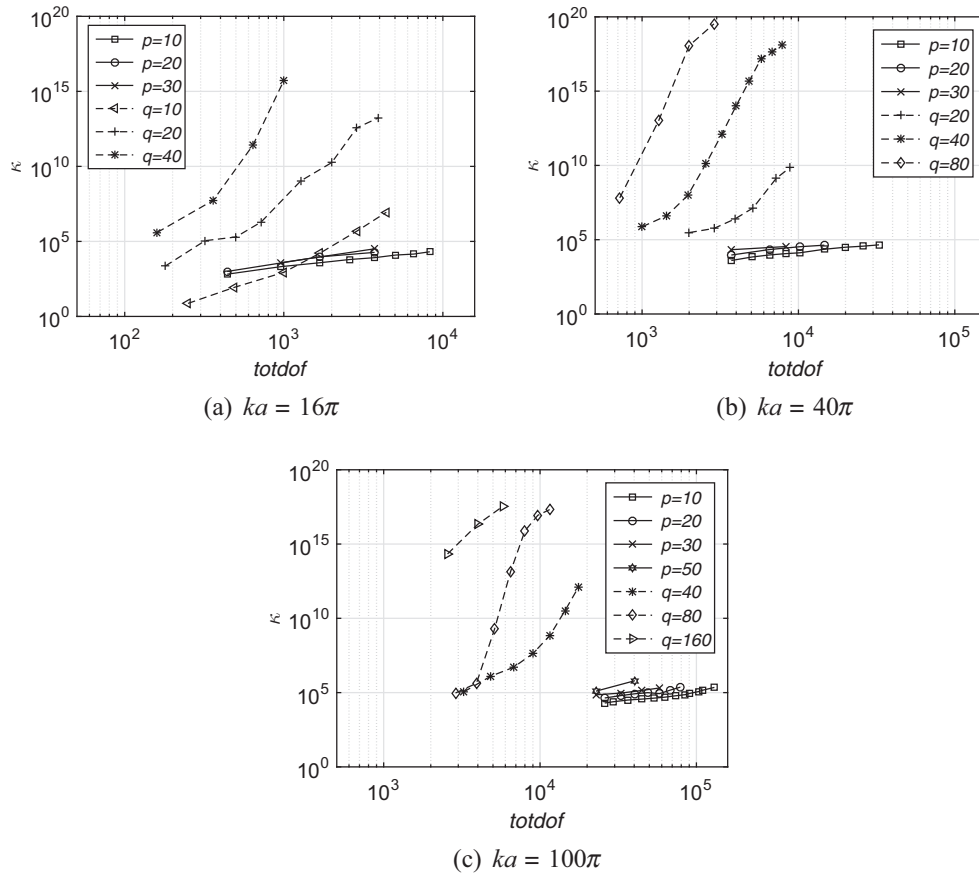
(c) $ka = 100\pi$

Fig. 2. Condition number for PUFEM and SEM for different values of the wave number.

plane waves is increased. In fact, ill-conditioning is an inherent feature of PUFEM but despite the high values of κ, PUFEM continues to provide good quality results with decreasing L_2-error as *totdof* increases through mesh refinement or by increasing the number q of approximating plane waves.

In Fig. 3, the total number of non-zero entries, *totnze*, indicating the storage requirements for the final system to solve is presented with respect to the total number of degrees of freedom, *totdof*, for the same parameters considered above. As expected, for both SEM and PUFEM, the total number of non-zero entries increases exponentially as h-refinement is carried out, for a given p or given q. Moreover, as p and q increase, *totnze* also increases due to the elementary matrices becoming larger, $(p+1) \times (p+1)$ for SEM and $4q \times 4q$ in PUFEM, with p and q. Nevertheless, as already noticed, while there are some comparable numbers between SEM and PUFEM for the wave number cases $ka = 16\pi$ and 40π, it is clear at the higher wave number $ka = 100\pi$ SEM requires more degrees of freedom and hence exhibits large numbers of non-zero entries to achieve similar quality of results as PUFEM.

In all numerical tests carried out above, the computational domain was meshed into uniform mesh grids with square elements of the same size. In the next numerical tests, the mesh grid is distorted such as shown in Fig. 4. A distortion ratio is defined by dividing the largest element edge by the smallest one in the same mesh grid. Therefore, Fig. 4(a) shows an undistorted mesh grid with the defined ratio equal to one, Fig. 4(b) represents an intermediate distortion case and Fig. 4(c) shows the extreme distortion for which the ratio is equal to 10. The mesh grids contain 25 elements. In the case of PUFEM, 4-node elements are used with q plane wave enrichment at each node. For SEM, each element contains $(p+1)^2$

nodes so that the interpolation functions are of degree p. The plane wave scattering problem dealt with above is considered again here, for $ka = 8\pi$ and 16π, with SEM and PUFEM for different orders p of the interpolation polynomials and numbers q of approximating plane waves, respectively. The L_2-error is shown in Fig. 5 as a function of the distortion ratio.

Overall, Fig. 5 shows that some of the results are affected by the increase of the distortion ratio and hence the L_2-error has increased, such as for SEM with $p = 10$ and PUFEM with $q = 20$, while others show a practically flat L_2-error, such as for SEM with $p = 20$ and PUFEM with $q = 40$. This is due to the change in the discretization level τ which varies with the distortion ratio. Indeed, for the undistorted mesh grid, the average number of degrees of freedom per wavelength is the same at all elements. It is about 6.7 for PUFEM with $q = 20$ and 12.7 for SEM with $p = 10$, for the case of $ka = 8\pi$. For this wave number, these levels are about 9.5 for PUFEM with $q = 40$ and 25.2 for SEM with $p = 20$. As the mesh is distorted, the average number of degrees of freedom per wavelength at element level will vary such that it is high in the small elements and low at the large ones. Therefore the L_2-error would be affected by the large elements incorporating less degrees of freedom per wavelength. As the wave number increased from 8π to 16π, leading to half of the above mentioned discretization levels, the L_2-error seems to be affected for SEM with $p = 10$ and PUFEM with $q = 20$, due to the lower number of degrees of freedom per wavelength within the large elements. However, for SEM with $p = 20$ and PUFEM with $q = 40$ the results remain practically unchanged thanks to the discretization levels which remained relatively high even for the large distorted elements.
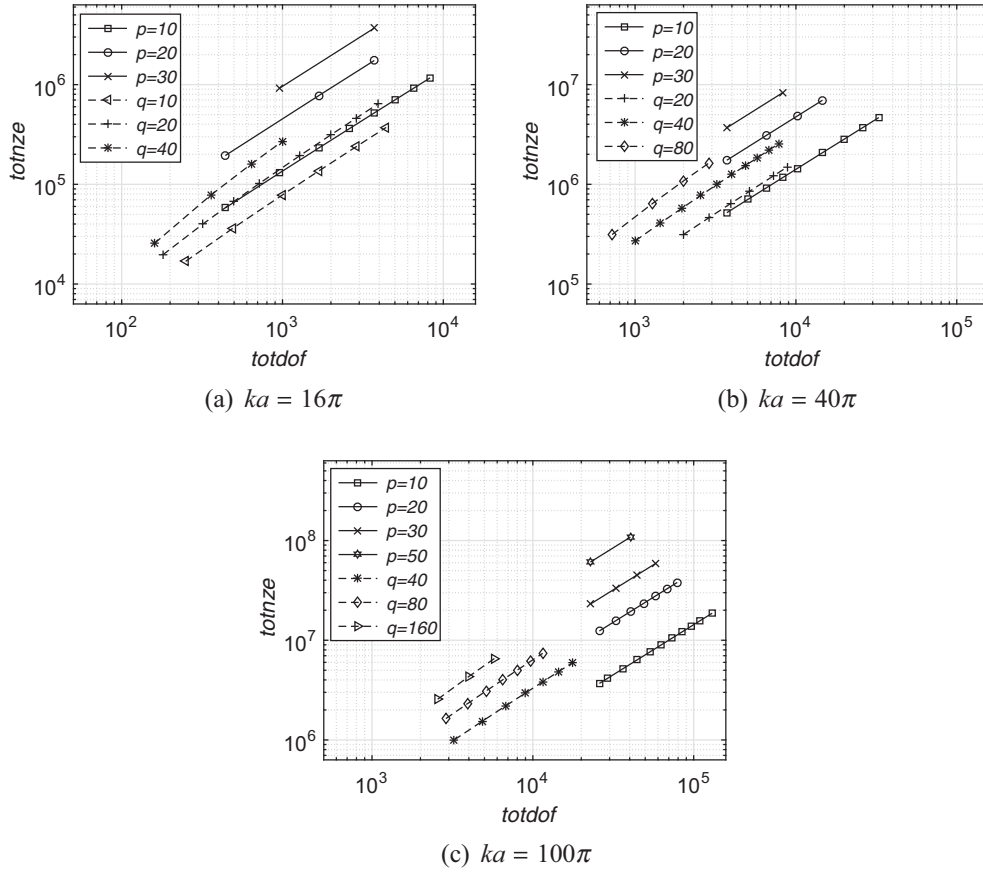
(a) $ka = 16\pi$ (b) $ka = 40\pi$

(c) $ka = 100\pi$

Fig. 3. Non-zero entries for PUFEM and SEM for different values of the wave number.
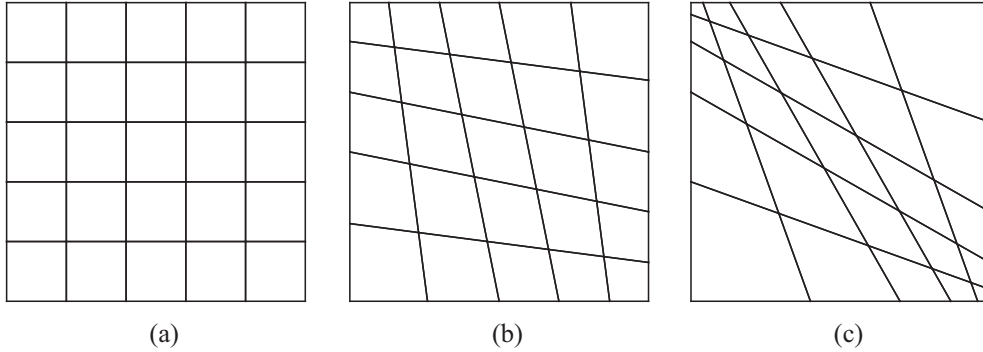

(a) (b) (c)

Fig. 4. (a) Undistorted mesh grid, (b) intermediate distortion and (c) extreme distortion.

3.2. Exponentially decaying wave problems

It is well known that the performance of wave-based methods tends to be reduced when dealing with problems involving evanescent waves. In this section, two further test cases of practical interest are considered. The first case deals with the propagation of waves in a duct with rigid walls, which involves propagating and decaying modes, and the second one involves evanescent waves.

3.2.1. Wave propagation in a duct

The first test example deals with the propagation of a wave in a duct with rigid walls. It is taken from Ref. [41]. The computational domain $\Omega = [0,2] \times [0,1]$ is considered with the Robin condition (2) on its boundary Γ through the source term g. The solution of the problem is given by

$$u(x,y) = \cos(\alpha\pi y)(B_1 e^{-ik_x x} + B_2 e^{ik_x x}), \qquad (17)$$

where $k_x = \sqrt{k^2 - (\alpha\pi)^2}$. For $k > \alpha\pi$, the solution exhibits propagating modes, otherwise, we are dealing with an evanescent wave problem. The coefficients B_1 and B_2 can be found by solving the equation

$$i\begin{pmatrix} k_x & -k_x \\ (k - k_x)e^{-2ik_x} & (k + k_x)e^{2ik_x} \end{pmatrix}\begin{pmatrix} B_1 \\ B_2 \end{pmatrix} = \begin{pmatrix} 1 \\ 0 \end{pmatrix}. \qquad (18)$$

In Ref. [41], the ultra weak variational formulation and PUFEM were assessed in solving the problem stated above for the wave numbers 20, 40 and 80 using mesh grids based on triangular elements. In this work, PUFEM and SEM are used on uniform mesh grids with square elements to solve the above problem for the wave numbers $ka = 40$,
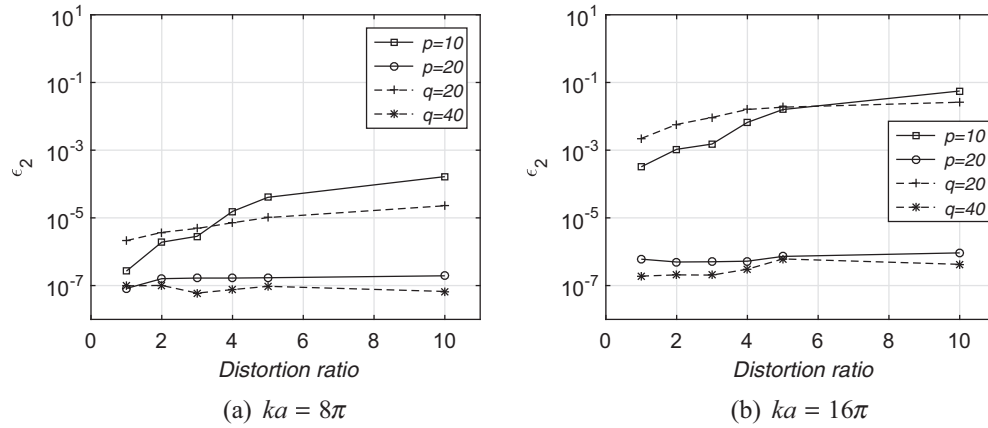
Fig. 5. Relative L_2-error for PUFEM and SEM for different values of the wave number on distorted mesh grids.

80 and 160. Here, the parameter a represents a unit of length such that ka is dimensionless. For each case of wave number, two different values of α, which give the highest-propagating mode and the lowest-evanescent mode, are considered. For illustration purpose, Fig. 6 shows the analytical solution (17) for $ka = 40$ with $\alpha = 12$ corresponding to a propagating wave and $\alpha = 13$ corresponding to an evanescent wave. Obviously, as k increases the values of α leading to propagating or evanescent modes increase as well.

To increase the discretization level τ, the mesh size is refined for the SEM approach while for PUFEM the number q of enriching plane waves is increased. This is an h-approach for SEM while for PUFEM it is a q-approach, equivalent to the p-approach. This is deliberately adopted because it is usual to adopt h-refinements in the case of SEM but for PUFEM it is more practical to keep the mesh grid of the computational domain unchanged and increase the number q of field enrichment functions.

For PUFEM, a mesh grid of 2 by 4 square elements is used for the wave numbers $ka = 40$ and 80, and a mesh grid with 4 by 8 square elements is used for $ka = 160$. Tables 1–3 display the computed L_2-error and the discretization level, presented between brackets, for the considered cases.

As expected, the error decreases as the mesh grid is refined for SEM with a given order p and by increasing the number q of enriching plane waves for PUFEM. This is valid for both values of α representing propagating and evanescent modes. For all cases, PUFEM requires less degrees of freedom per wavelength in comparison

to SEM in order to reach a prescribed accuracy. While SEM requires more degrees of freedom per wavelength, this number decreases as p increases. For example, in the case of $ka = 40$, the lowest PUFEM L_2-errors are 1.9×10^{-6} and 1.2×10^{-5}, for propagating and evanescent modes respectively, and are both obtained with $\tau = 3.0$. The nearest SEM discretization level is 3.4 with $p = 30$ and the L_2-errors are 3.8×10^{-5} and 2.0×10^{-4}, for propagating and evanescent modes respectively. At the higher frequency $ka = 80$, the lowest PUFEM L_2-errors are obtained with $\tau = 1.9$. Such errors may be obtained with SEM with τ greater than 3 even with $p = 30$, for both propagating and evanescent waves. This also applies to the highest frequency case $ka = 160$ where the L_2-error of 3.0×10^{-5} for the propagating mode is obtained with $\tau = 1.9$ using PUFEM. An equivalent L_2-error requires more than 3 degrees of freedom per wavelength using SEM. A similar remark is drawn for the evanescent mode too.

For all considered wave numbers, the results also show that the solution requires more degrees of freedom per wavelength to reach a certain accuracy for the evanescent wave problem in comparison to the propagating mode problem. For example, in the case of $ka = 40$, PUFEM leads to results with $\epsilon_2 = 1.2 \times 10^{-2}$ and 8.8×10^{-4} with $\tau = 1.9$ and 2.4, respectively, in the case of the propagating mode. These errors increased to about 3.9×10^{-1} and 4.1×10^{-2}, respectively, in the case of the evanescent mode. This observation is also valid for the SEM approach.
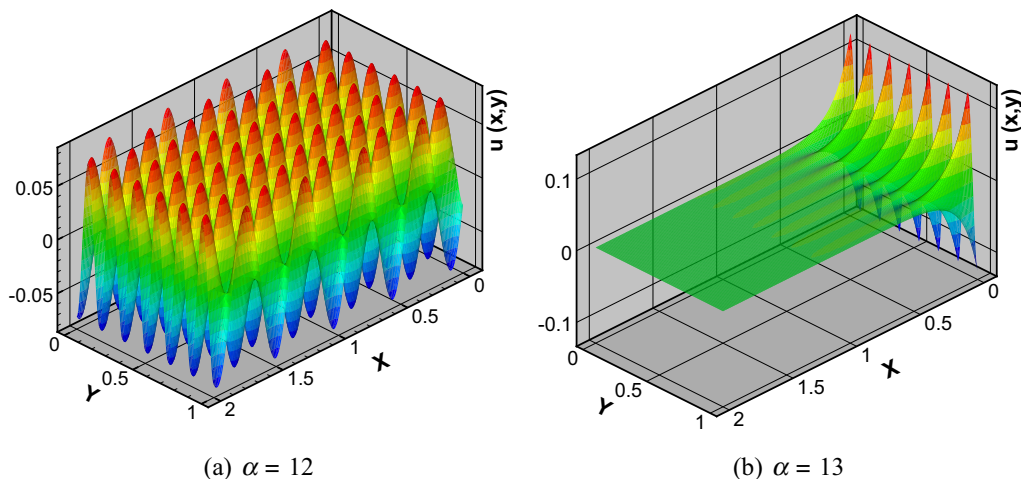

Fig. 6. Waves in a duct for $ka = 40$, (a) propagating mode for $\alpha = 12$ and (b) evanescent mode for $\alpha = 13$.

Table 1
Wave propagation in a duct. Relative L_2-error and discretization level for SEM and PUFEM for $ka = 40$.

	SEM			PUFEM
	$p = 10$	$p = 20$	$p = 30$	
$\alpha = 12$	3.8×10^{-5} (5.7)	2.0×10^{-6} (4.6)	3.8×10^{-5} (3.4)	1.2×10^{-2} (1.9)
	5.0×10^{-7} (9.0)	6.0×10^{-7} (6.8)	9.0×10^{-7} (6.8)	8.8×10^{-4} (2.4)
	5.0×10^{-7} (11.2)	5.0×10^{-7} (11.2)	7.0×10^{-7} (10.1)	5.6×10^{-5} (2.7)
	5.0×10^{-7} (13.4)	6.0×10^{-7} (13.4)	5.0×10^{-7} (13.4)	1.9×10^{-6} (3.0)
$\alpha = 13$	8.7×10^{-5} (5.7)	8.5×10^{-6} (4.6)	2.0×10^{-4} (3.4)	3.9×10^{-1} (1.9)
	1.1×10^{-6} (9.0)	1.0×10^{-6} (6.8)	1.2×10^{-6} (6.8)	4.1×10^{-2} (2.4)
	1.0×10^{-6} (11.2)	1.0×10^{-6} (11.2)	1.0×10^{-6} (10.1)	4.1×10^{-3} (2.7)
	9.0×10^{-7} (13.4)	1.0×10^{-6} (13.4)	1.0×10^{-6} (13.4)	1.2×10^{-5} (3.0)

Table 2
Wave propagation in a duct. Relative L_2-error and discretization level for SEM and PUFEM for $ka = 80$.

	SEM			PUFEM
	$p = 10$	$p = 20$	$p = 30$	
$\alpha = 25$	5.8×10^{-4} (4.5)	7.2×10^{-4} (3.4)	6.0×10^{-5} (3.4)	1.0×10^{-2} (1.5)
	2.0×10^{-6} (7.3)	3.0×10^{-5} (5.6)	1.2×10^{-6} (5.1)	7.6×10^{-3} (1.7)
	1.0×10^{-6} (8.4)	1.0×10^{-6} (7.8)	1.0×10^{-6} (6.7)	2.8×10^{-4} (1.8)
	9.0×10^{-7} (9.5)	1.0×10^{-6} (8.9)	1.0×10^{-6} (8.4)	2.5×10^{-5} (1.9)
$\alpha = 26$	8.5×10^{-4} (4.5)	1.4×10^{-4} (3.4)	2.1×10^{-4} (3.4)	1.9×10^{-1} (1.5)
	7.8×10^{-6} (7.3)	7.1×10^{-6} (5.6)	2.1×10^{-6} (5.1)	4.9×10^{-2} (1.7)
	1.7×10^{-6} (8.4)	1.7×10^{-6} (7.8)	1.9×10^{-6} (6.7)	8.5×10^{-3} (1.8)
	1.7×10^{-6} (9.5)	1.7×10^{-6} (8.9)	1.7×10^{-6} (8.4)	2.8×10^{-4} (1.9)

Table 3
Wave propagation in a duct. Relative L_2-error and discretization level for SEM and PUFEM for $ka = 160$.

	SEM			PUFEM
	$p = 10$	$p = 20$	$p = 30$	
$\alpha = 50$	5.9×10^{-3} (3.6)	8.4×10^{-3} (2.8)	5.1×10^{-2} (2.5)	1.7×10^{-2} (1.6)
	5.9×10^{-5} (5.6)	4.9×10^{-5} (3.9)	6.1×10^{-5} (3.4)	2.5×10^{-3} (1.7)
	1.9×10^{-5} (6.4)	1.5×10^{-5} (4.5)	1.3×10^{-5} (4.2)	1.2×10^{-4} (1.8)
	1.4×10^{-5} (8.4)	1.4×10^{-5} (5.0)	1.4×10^{-5} (5.0)	3.0×10^{-5} (1.9)
$\alpha = 51$	6.9×10^{-3} (3.6)	2.5×10^{-2} (2.8)	1.0×10^{-1} (2.5)	2.3×10^{-3} (1.6)
	7.5×10^{-5} (5.6)	7.2×10^{-5} (3.9)	9.9×10^{-5} (3.4)	9.6×10^{-4} (1.7)
	2.9×10^{-5} (6.4)	2.4×10^{-5} (4.5)	2.3×10^{-5} (4.2)	4.5×10^{-5} (1.8)
	2.4×10^{-5} (8.4)	2.4×10^{-5} (5.0)	2.4×10^{-5} (5.0)	1.4×10^{-4} (1.9)

3.2.2. Evanescent wave case

The second test case is taken form reference [43]. It deals with the numerical solution of an evanescent wave problem in a square domain $\Omega = [-1, 1] \times [-1, 1]$, on the boundary of which the Robin condition (2) is applied with the solution of the problem being

$$u = e^{i\beta k y} e^{-k\sqrt{\beta^2 - 1}(x+1)}. \tag{19}$$

The evanescent wave (19) propagates in the y-direction and decays in the x-direction depending on the values of $\beta > 1$ and k. In [43], the solution was obtained using the Ultra Weak Variational Formulation with either plane waves or Bessel basis functions over a uniform triangular mesh grid.

In this work, the same problem is revisited and solved at relatively high frequencies $ka = 25$, 50 and 100. For such values of ka, the parameter β is chosen to be equal to 1.001 and 1.5 to consider different rates of decay in the x-direction. This is depicted in Fig. 7, which shows the behaviour of the model solution given in expression (19) for $ka = 25$ and 100. It is obvious that for the higher wave number ka more wavelengths are displayed in the y-direction and that for the higher coefficient β a shaper decay occur in the x-direction, which represent challenging test cases.

Table 4 summarises the results in terms of the L_2-error and the discretization level, presented between brackets, for the three cases of the wave number. For SEM, uniform mesh grids are considered and for PUFEM, a mesh grid of 2 by 2 square elements is used for the wave numbers $ka = 25$ and 50, and a mesh grid with 4 by 4 square elements is used for $ka = 100$. The same approach used for the case of wave propagation in a duct is also followed here *i.e.* to increase the discretization level, mesh refinements are carried out for SEM while for PUFEM the mesh grid is kept unchanged and the number of approximating plane waves is increased. Again, this is deliberately adopted for the reason stated earlier. Moreover, for PUFEM, on top of the plane wave enrichment results, mentioned by PW, plane waves and evanescent waves enrichments, noted by PW + EW are also considered, for which two exponentially decaying waves are added to the plane waves. These are chosen to be $e^{i\beta k y} e^{-k\sqrt{\beta^2 - 1}(x+1)}$ and $e^{-i\beta k y} e^{-k\sqrt{\beta^2 - 1}(x+1)}$. Note that the discretization level τ remains practically unchanged as it is the second digit of τ which is affected.

In general, the results show that increasing the discretization level τ improves the L_2-error for both approaches, SEM and PUFEM with PW. For SEM, as the order p increases, the discretization level τ required to achieve a prescribed accuracy decreases but PUFEM with PW seems to provide similar quality results for significantly lower values of the discretization level τ. For example, for $ka = 25$, PUFEM with PW provides an error of order 10^{-6} with $\tau = 2.7$ whereas an error of the same order is achieved with $\tau = 10.2$ for $p = 10$ and with $\tau = 7.7$ for $p = 20$ and 30. For
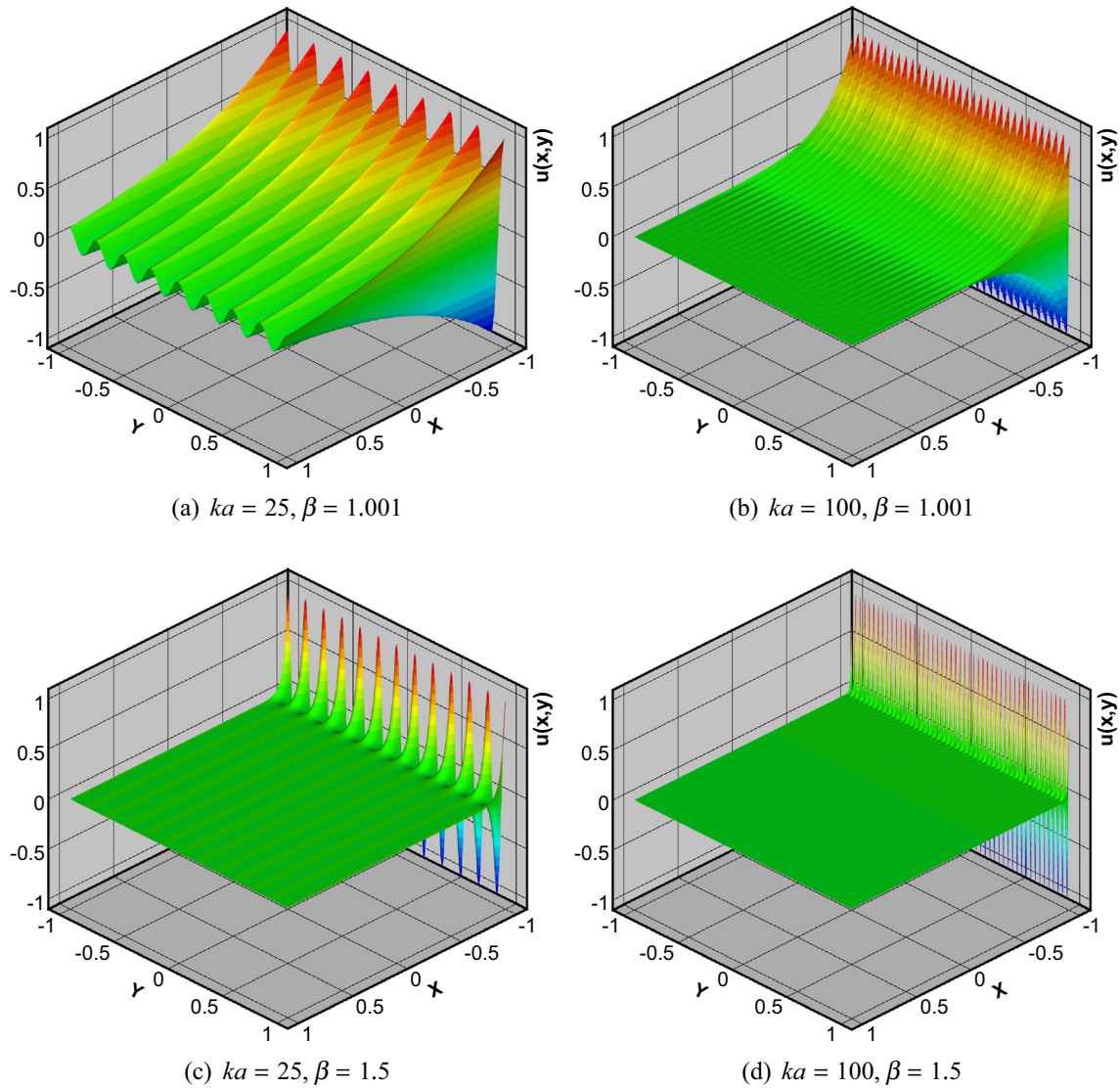
(a) $ka = 25, \beta = 1.001$

(b) $ka = 100, \beta = 1.001$

(c) $ka = 25, \beta = 1.5$

(d) $ka = 100, \beta = 1.5$

Fig. 7. Evanescent wave variations in the computational domain for different values of ka and β.

Table 4
Evanescent wave test case. Relative L_2-error and discretization level for SEM and PUFEM for $ka = 25, 50, 100$ and $\beta = 1.001$.

	SEM			PUFEM	
$p = 10$	$p = 20$	$p = 30$		PW	PW + EW
		$ka = 25$			
7.0×10^{-4} (6.4)	3.3×10^{-4} (5.2)	1.5×10^{-2} (3.9)		8.8×10^{-2} (2.1)	1.4×10^{-5} (2.1)
5.3×10^{-6} (10.2)	1.5×10^{-6} (7.7)	1.3×10^{-6} (7.7)		9.0×10^{-5} (2.4)	3.2×10^{-6} (2.4)
1.0×10^{-7} (15.2)	2.0×10^{-7} (12.7)	9.0×10^{-7} (11.4)		3.2×10^{-6} (2.7)	3.2×10^{-6} (2.7)
8.0×10^{-8} (22.8)	9.0×10^{-8} (17.7)	5.0×10^{-7} (15.2)		3.2×10^{-6} (3.0)	3.2×10^{-6} (3.0)
		$ka = 50$			
3.4×10^{-2} (4.5)	4.4×10^{-2} (3.8)	1.5×10^{-2} (3.8)		1.6×10^{-2} (1.5)	6.4×10^{-6} (1.5)
5.3×10^{-6} (10.1)	6.1×10^{-6} (6.4)	2.5×10^{-6} (5.7)		8.2×10^{-4} (1.6)	6.4×10^{-6} (1.6)
1.5×10^{-6} (11.4)	1.6×10^{-6} (7.6)	2.3×10^{-6} (7.6)		8.1×10^{-6} (1.7)	7.1×10^{-6} (1.7)
2.0×10^{-7} (13.9)	2.0×10^{-7} (11.4)	9.0×10^{-7} (9.5)		8.0×10^{-6} (1.8)	7.5×10^{-6} (1.8)
		$ka = 100$			
4.3×10^{-3} (5.4)	3.3×10^{-3} (4.4)	1.8×10^{-2} (3.8)		1.7×10^{-2} (1.3)	1.2×10^{-5} (1.3)
1.2×10^{-3} (6.0)	4.0×10^{-5} (5.7)	9.5×10^{-5} (4.7)		1.3×10^{-3} (1.5)	1.2×10^{-5} (1.5)
1.7×10^{-4} (7.3)	6.2×10^{-6} (6.3)	2.6×10^{-6} (5.7)		7.9×10^{-4} (1.6)	2.1×10^{-5} (1.6)
3.2×10^{-5} (8.5)	1.9×10^{-6} (7.6)	2.7×10^{-6} (6.6)		1.3×10^{-5} (1.8)	1.3×10^{-5} (1.8)

$ka = 50$, PUFEM with PW provides an error of order 10^{-6} with $\tau = 1.7$, a number which is almost three times lower than that required for $p = 30$ in order to achieve the same L_2-error. Similarly,

for $ka = 100$ PUFEM with PW and $\tau = 1.8$ provides an error of 10^{-5} whereas the same error is provided with SEM at significantly higher numbers of τ.

For PUFEM with PW + EW, the results show lower L_2-errors at very low levels of the discretization level τ, in comparison to the results of PUFEM with PW. It is obvious that the incorporation of the two evanescent waves in the wave field enrichment has significantly improved the performance of the model for the lowest values of the discretization level. For example, in the case of $ka = 25$, PUFEM with PW + EW provides an L_2-error of 1.4×10^{-5} with $\tau = 2.1$ while PUFEM with PW and with the same discretization level provides an L_2-error of 8.8×10^{-2}. This improvement is noticed in all cases of wave numbers. It is also noticed that further increasing the number of approximating plane waves does not reduce the L_2-error. This is due to the fact that the good performance of PUFEM to deal with evanescent wave problems is due to the exponentially decaying waves added to the approximating plane waves. It is also known that PUFEM L_2-errors stagnate after reaching a certain level of accuracy and further increasing τ does not improve the error. This is observed for PUFEM with PW in the case of $ka = 25$ for $\tau = 2.7$ and 3, and in the case of $ka = 50$ for $\tau = 1.7$ and 1.8. Overall, the lowest levels of L_2-error are achieved by the SEM approach but with significantly higher discretization levels.

The same problem is considered again but this time with the coefficient $\beta = 1.5$. This leads to a very sharp exponential decrease of the evanescent wave given by expression (19) and hence it is numerically more challenging than that corresponding to $\beta = 1.001$.

Table 5 shows the obtained values of the L_2-error with the corresponding discretization levels for the wave number $ka = 25, 50$ and 100. For SEM, only the order $p = 30$ is considered and for PUFEM both equally distributed progressive plane waves and the two exponentially decaying waves considered above are used in the approximating field enrichment (PW + EW). It is worth noting that PUFEM with PW did not produce good quality results for this case of the coefficient $\beta = 1.5$ representing a very sharp decay of the evanescent wave (Fig. 7). SEM results show a progressive decrease of the L_2-error as the discretization level increases. For less than about 4 degrees of freedom per wavelength, SEM results are not of good quality. In the case PUFEM, with PW + EW, all results display L_2-errors of the order of 10^{-5} or 10^{-6} even for the lowest discretization level, $\tau = 1.3$, thanks to incorporating exponentially decaying waves in the enrichment field. The L_2-error seem to be stagnating in spite of the increase of τ through the increase of the number of approximating progressive plane waves, which are less crucial than the exponentially decaying waves for this problem. In the above test case, the inclusion of the evanescent

wave (19) in the wave basis leads to better results because it corresponds to the exact solution. In a general case, where no a priori knowledge of the solution is available, it is difficult to propose a robust model to efficiently solve the problem. In such case, the use of polynomial-based elements would be more practical.

4. Conclusions

In this paper, two high order finite element approaches are used to solve wave problems governed by the Helmholtz equation in two dimensions. In one approach, referred to as SEM, the Lagrangian polynomial based finite elements with Chebyshev-Gauss-Lobatto nodal distribution are considered with high orders, up to $p = 50$. In the other approach, PUFEM is considered with oscillatory functions in the form of progressive plane waves or including exponentially decaying waves. The performance of each approach is assessed in terms of results quality and required degrees of freedom per wavelength. The condition number, the total number of required storage locations and the total number of non-zero entries in the final system to solve are also compared.

For the considered problems, the results show that PUFEM provides good quality results with a low number of degrees of freedom per wavelength, especially for relatively high frequencies where the element size incorporates many wavelengths. Good quality results are obtained with less than 2 degrees of freedom per wavelength. In such cases, the final system to solve is drastically reduced in comparison to SEM and hence the number of storage locations is also reduced. However, it is also shown that further increasing the discretization level by increasing the number of enriching plane waves does not always enhance the results beyond a certain level due to the ill-conditioning issue which is inherent to the plane wave enrichment technique.

For SEM, as the order p increases, the required number of degrees of freedom per wavelength to provide results with a prescribed level of accuracy decreases and, in general, it remains higher than that required by PUFEM. This is especially seen at the highest considered order for SEM, $p = 50$, and high number q of enrichment functions for PUFEM. At a lower order, for example $p = 10$ or 20, SEM may lead to a similar performance obtained by PUFEM with low number of enriching plane waves, such as $q = 10$ or 20.

For problems involving evanescent waves, SEM provides good quality results but again with a higher discretization level in comparison to PUFEM. For the latter approach, incorporating exponentially decaying waves in the enrichment field significantly enhances its performance, especially for cases with a sharp decay where the efficiency of PUFEM with progressive plane wave enrichment is significantly reduced.

In view of the results presented in this work and given the cumbersome task of creating high order elements mesh grids, especially for engineering problems of industrial scale, it seems more practical to use low order elements and incorporate field enrichment. Moreover, it is always possible for practitioners to choose the number and type of enrichment functions for a given frequency and mesh size to obtain good quality results while keeping the condition number within acceptable limits. However, if the wave field exhibits sharp decay behaviour and no a-priori knowledge of the solution is available, then polynomial-based elements would be a more practical option.

Table 5
Evanescent wave test case. Relative L_2-error and discretization level for SEM and PUFEM for $ka = 25, 50, 100$ and $\beta = 1.5$.

SEM $p = 30$	PUFEM PW + EW
ka = 25	
7.5×10^{-1} (3.9)	2.2×10^{-6} (2.1)
1.8×10^{-5} (7.7)	1.6×10^{-6} (2.4)
9.4×10^{-7} (11.4)	1.6×10^{-6} (2.7)
6.0×10^{-7} (15.2)	1.7×10^{-6} (3.0)
ka = 50	
7.5×10^{-1} (3.8)	5.2×10^{-6} (1.5)
1.2×10^{-2} (5.7)	5.3×10^{-6} (1.6)
1.8×10^{-5} (7.6)	6.9×10^{-6} (1.7)
2.0×10^{-6} (9.5)	4.5×10^{-6} (1.8)
ka = 100	
7.5×10^{-1} (3.8)	7.7×10^{-5} (1.3)
2.4×10^{-1} (4.7)	2.6×10^{-5} (1.5)
1.2×10^{-2} (5.7)	1.2×10^{-5} (1.6)
4.4×10^{-4} (6.6)	6.4×10^{-5} (1.8)

References

[1] Deraemaeker A, Babuška I, Bouillard P. Dispersion and pollution of the FEM solution for the helmholtz equation in one, two and three dimensions. Int J Numer Meth Eng 1999;46(4):471–99.

[2] El Kacimi A, Laghrouche O. Numerical modelling of elastic wave scattering in frequency domain by the partition of unity finite element method. Int J Numer Meth Eng 2009;77(12):1646–69.

[3] Gillman A, Djellouli R, Amara M. A mixed hybrid formulation based on oscillated finite element polynomials for solving helmholtz problems. J Comput Appl Math 2007;204(2):515–25.

[4] Pluymers B, Van Hal B, Vandepitte D, Desmet W. Trefftz-based methods for time-harmonic acoustics. Arch Comput Meth Eng 2007;14(4):343–81.

[5] Peter Bettess, Joseph Shirron, Omar Laghrouche, Bernard Peseux, Rie Sugimoto, Jon Trevelyan. A numerical integration scheme for special finite elements for the helmholtz equation. Int J Numer Meth Eng 2003;56(4):531–52.

[6] Farhat C, Harari I, Franca LP. The discontinuous enrichment method. Comp Meth Appl Mech Eng 2001;190(48):6455–79.

[7] Geuzaine C, Bedrossian J, Antoine X. An amplitude formulation to reduce the pollution error in the finite element solution of time-harmonic scattering problems. IEEE Trans Magnet 2008;44(6):782–5.

[8] Willberg C, Duczek S, Perez JMV, Schmicker D, Gabbert U. Comparison of different higher order finite element schemes for the simulation of lamb waves. Comp Meth Appl Mech Eng 2012;241:246–61.

[9] Perrey-Debain E, Laghrouche O, Bettess P, Trevelyan J. Plane-wave basis finite elements and boundary elements for three-dimensional wave scattering. Philos Trans R Soc Lond A: Math, Phys Eng Sci 2004;362(1816):561–77.

[10] A El Kacimi, O Laghrouche. Improvement of PUFEM for the numerical solution of high-frequency elastic wave scattering on unstructured triangular mesh grids. Int J Numer Meth Eng 2010;84(3):330–50.

[11] Ihlenburg F, Babuška I. Finite element solution of the helmholtz equation with high wave number part i: the h-version of the FEM. Comp Math Appl 1995;30 (9):9–37.

[12] Charbel Farhat, Radek Tezaur, Paul Weidemann-Goiran. Higher-order extensions of a discontinuous Galerkin method for mid-frequency helmholtz problems. Int J Numer Meth Eng 2004;61(11):1938–56.

[13] Giorgiani G, Modesto D, Fernández-Méndez S, Huerta A. High-order continuous and discontinuous Galerkin methods for wave problems. Int J Numer Meth Fluids 2013;73(10):883–903.

[14] Srinivasan Gopalakrishnan, Abir Chakraborty, Debiprosad Roy Mahapatra. Spectral finite element method: wave propagation, diagnostics and control in anisotropic and inhomogeneous structures. Springer Science & Business Media; 2007.

[15] Bériot H, Prinn A, Gabard G. Efficient implementation of high-order finite elements for Helmholtz problems. Int J Numer Meth Eng 2015.

[16] Bériot H, Gabard G, Perrey-Debain E. Analysis of high-order finite elements for convected wave propagation. Int J Numer Meth Eng 2013;96(11):665–88.

[17] Ralf Hiptmair, Andrea Moiola, Ilaria Perugia. A survey of Trefftz methods for the helmholtz equation. arXiv preprint arXiv:1506.04521; 2015.

[18] Babuska I, Melenk JM. The partition of unity finite element method, Technical report. DTIC Document; 1995.

[19] Chazot JD, Perrey-Debain E, Nennig B. The partition of unity finite element method for the simulation of waves in air and poroelastic media. J Acoust Soc Am 2014;135(2):724–33.

[20] Melenk JM. On generalized finite element methods, PhD thesis. The University of Maryland; 1995.

[21] George Karniadakis, Spencer Sherwin. Spectral/hp element methods for computational fluid dynamics. Oxford University Press; 2013.

[22] Zhang L, Tezaur R, Farhat C. The discontinuous enrichment method for elastic wave propagation in the medium-frequency regime. Int J Numer Meth Eng 2006;66(13):2086–114.

[23] Alice Lieu, Gwénaël Gabard, Hadrien Bériot. A comparison of high-order polynomial and wave-based methods for helmholtz problems. J Comput Phys 2016;321:105–25.

[24] Amara M, Calandra H, Dejllouli R, Grigoroscuta-Strugaru M. A stable discontinuous Galerkin-type method for solving efficiently helmholtz problems. Comp Struct 2012;106:258–72.

[25] Peake MJ, Trevelyan J, Coates G. Extended isogeometric boundary element method (XIBEM) for two-dimensional helmholtz problems. Comp Meth Appl Mech Eng 2013;259:93–102.

[26] Cessenat O, Després B. Application of an ultra weak variational formulation of elliptic PDES to the two-dimensional Helmholtz problem. SIAM J Numer Anal 1998;35(1):255–99.

[27] Cessenat O, Després B. Using plane waves as base functions for solving time harmonic equations with the ultra weak variational formulation. J Comput Acoust 2003;11(02):227–38.

[28] Laghrouche O, Mohamed MS. Locally enriched finite elements for the helmholtz equation in two dimensions. Comp Struct 2010;88(23):1469–73.

[29] Laghrouche O, Bettess P. Short wave modelling using special finite elements. J Comput Acoust 2000;8(01):189–210.

[30] Laghrouche O, Bettess P, Perrey-Debain E, Trevelyan J. Wave interpolation finite elements for helmholtz problems with jumps in the wave speed. Comp Meth Appl Mech Eng 2005;194(2):367–81.

[31] Laghrouche O, Bettess P, Astley RJ. Modelling of short wave diffraction problems using approximating systems of plane waves. Int J Numer Meth Eng 2002;54(10):1501–33.

[32] Bettess P, Jacqueline A. A profile matrix solver with built-in constraint facility. Eng Comput 1986;3(3):209–16.

[33] Monk P, Wang DQ. A least-squares method for the helmholtz equation. Comp Meth Appl Mech Eng 1999;175(1):121–36.

[34] Anthony T Patera. A spectral element method for fluid dynamics: laminar flow in a channel expansion. J Comput Phys 1984;54(3):468–88.

[35] Constantine Pozrikidis. Introduction to finite and spectral element methods using MATLAB. CRC Press; 2005.

[36] Tezaur R, Farhat C. Three-dimensional discontinuous Galerkin elements with plane waves and lagrange multipliers for the solution of mid-frequency Helmholtz problems. Int J Numer Meth Eng 2006;66(5):796–815.

[37] Astley RJ, Gamallo P. Special short wave elements for flow acoustics. Comp Meth Appl Mech Eng 2005;194(2):341–53.

[38] Petersen S, Dreyer D, von Estorff O. Assessment of finite and spectral element shape functions for efficient iterative simulations of interior acoustics. Comp Meth Appl Mech Eng 2006;195(44):6463–78.

[39] Pavel Solin, Karel Segeth, Ivo Dolezel. Higher-order finite element methods. CRC Press; 2003.

[40] Huttunen T, Kaipio JP, Monk P. An ultra-weak method for acoustic fluid-solid interaction. J Comput Appl Math 2008;213(1):166–85.

[41] Huttunen T, Gamallo P, Astley RJ. Comparison of two wave element methods for the Helmholtz problem. Commun Numer Meth Eng 2009;25(1):35–52.

[42] Huttunen T, Monk P, Collino F, Kaipio JP. The ultra-weak variational formulation for elastic wave problems. SIAM J Scient Comput 2004;25 (5):1717–42.

[43] Luostari T, Huttunen T, Monk P. The ultra weak variational formulation using bessel basis functions. Commun Comput Phys 2012;11(2):400.

[44] Strouboulis T, Babuška I, Copps K. The design and analysis of the generalized finite element method. Comp Meth Appl Mech Eng 2000;181(1):43–69.

[45] Strouboulis T, Copps K, Babuska I. The generalized finite element method: an example of its implementation and illustration of its performance. Int J Numer Meth Eng 2000;47(8):1401–17.

[46] Strouboulis T, Hidajat R, Babuška I. The generalized finite element method for helmholtz equation. Part ii: effect of choice of handbook functions, error due to absorbing boundary conditions and its assessment. Comp Meth Appl Mech Eng 2008;197(5):364–80.